Polymer Testing 65 (2018) 429–439

Contents lists available at ScienceDirect

Polymer Testing

journal homepage: www.elsevier.com/locate/polytest

Material Properties

On the key role of SiO_2@POSS hybrid filler in tailoring networking and interfaces in rubber nanocomposites

Matteo Redaelli[a], Massimiliano D'Arienzo[a,*], Jiri Brus[b], Barbara Di Credico[a], Marco Geppi[c], Luca Giannini[d], Libor Matejka[b], Francesca Martini[c], Francesco Panattoni[c], Milena Spirkova[b], Miroslav Šlouf[b], Roberto Scotti[a], Franca Morazzoni[a]

[a] Dept. of Materials Science, INSTM, University of Milano-Bicocca, Via R. Cozzi, 55, 20125 Milano, Italy
[b] Institute of Macromolecular Chemistry, Academy of Sciences of the Czech Republic, Heyrovsky Sq. 2, 162 06 Prague 6, Czech Republic
[c] Dipartimento di Chimica e Chimica Industriale, Università di Pisa, via G. Moruzzi 13, 56124 Pisa, Italy
[d] Pirelli Tyre SpA, Viale Sarca, 222, 20126 Milano, Italy

ARTICLE INFO

Keywords:
Rubber nanocomposites
Hybrid materials
POSS
Nanofillers

ABSTRACT

The present study provides a comprehensive investigation at the micro and nanoscale of the interface between hybrid SiO_2@POSS nanofiller, where silica nanoparticles (NPs) and POSS nanocages are intimately interconnected, and Styrene Butadiene Rubber (SBR). SEM and AFM inspection and, more in depth, solid state ^1H NMR revealed a remarkable fraction of rigid rubber close to the SiO_2@POSS surfaces, which increases with the curing temperature. Instead, a reduced amount of immobilized rubber was detected for SBR/SiO_2 + POSS nanocomposites, obtained by simply mixing SBR, SiO_2 and POSS.

The results allowed us to propose a model for the network formation in C-SBR/SiO_2@POSS.

This is based on the progressive activation by dicumylperoxide (DCP) of the methacryl functionalities of POSS nanounits which, being closely connected to SiO_2 NPs in SiO_2@POSS, promote crosslinking in proximity of the filler surfaces, and lead to the generation of a tight network strongly bonded to the rubber chains.

1. Introduction

Rubber nanocomposites are important technological materials that received increasing interest in recent decades owing to their tunable mechanical properties and broad applications [1–3]. In particular, rubber nanocomposites are the dominating materials in tires due to their excellent mechanical features, dimensional stability, flame retardancy, improved scratch and mar resistance, superior thermal and processing properties, reduced warpage of components and enhanced impact resistance [1–8]. The extent of these properties depends on the viscoelastic properties of the rubber composites, which are related to filler type and amount, filler particle size and shape (aspect ratio), particle aggregation in the matrix (filler-filler interaction) and interfacial adhesion between filler and polymer chains (filler-rubber interaction). These characteristics determine the formation of a percolative filler network in the rubber matrix, which is essential for providing effective reinforcement [9–11].

In this respect, we have recently reported [12] on the promising properties of polyhedral oligomeric silsesquioxanes (POSS) [13–15] used as molecular nanofillers together with SiO_2 nanoparticles (NPs). They were able to enhance simultaneously the filler networking and the filler-rubber interaction in rubber composites for tires.

The hybrid NPs were then used to prepare, by ex-situ blending, styrene butadiene rubber (SBR) nanocomposites which, after DCP curing, display outstanding mechanical strength and reduced hysteresis, becoming very suitable for application in tires. Moreover, comparing the performance of SBR/SiO_2@POSS to that of composites prepared by mixtures of SiO_2 and OctaMethacrylPOSS in the polymer matrix (SBR/SiO_2 + POSS), showed that the functionalization of silica surface with POSS determines a more positive effect on the modulus and reduces the hysteresis. These properties have been associated so far with the peculiar hybrid structure of SiO_2@POSS filler, in which silica NPs aggregates are partially interconnected and surrounded by a thin shell of POSS nanounits which, thanks to their high number of reactive functionalities, seem to promote the formation of “sticky regions” among the silica aggregates and, consequently, a tight filler network wherein rubber is immobilized [12].

Nevertheless, further morphological and physico-chemical evidence should be provided in order to explain, at the molecular level, the filler-rubber interactions occurring in the presence of SiO_2@POSS hybrid NPs

* Corresponding author.
E-mail addresses: m.redaelli19@campus.unimib.it (M. Redaelli), massimiliano.darienzo@unimib.it (M. D'Arienzo).

https://doi.org/10.1016/j.polymertesting.2017.12.022
Received 25 October 2017; Accepted 20 December 2017
Available online 24 December 2017
0142-9418/

and their role in modulating network formation and composite mechanical properties.

With this aim, the present study provides a comprehensive investigation at the micro and nanoscale of the interface between SiO_2@POSS and polymer chains, checking the filler adhesion in cured SBR/SiO_2@POSS composites by Scanning Electron Microscopy (SEM) and Atomic Force Microscopy (AFM) [16–19], and monitoring the changes in the rubber segmental dynamics by both low-field and high-field solid state Nuclear Magnetic Resonance spectroscopy (^{1}H-NMR) [11,20–27], as well as in comparison to the SBR/SiO_2 + POSS system. In this regard, solid state NMR spectroscopy provides clear information about the changes in polymer chain structure and dynamics, and its application in the study of rubber nanocomposites can afford in depth information on the nature and strength of the interfacial interaction between the elastomer blocks and filler nanounits in the final materials.

As both the filler distribution and networking are clearly influenced by the curing with DCP, which activates the POSS functionalities, the interfacial properties of the composites have also been evaluated after curing at increasing temperatures, i.e. starting when the peroxide is in principle less reactive and the curing process is at the early stages, toward the optimum conditions at which it is surely active and the curing is nearly complete [28].

Finally, the macroscopic properties of the composites have been assessed by determining their curing profiles and their mechanical behavior by Dynamic Mechanical Thermal Analysis (DMTA) and tensile stress–strain tests, which allowed us to evaluate their performance under a range of deformations [29,30].

2. Experimental

2.1. Materials

SiO_2@POSS synthesis: Silica Rhodia Zeosil MP1165; OctaMethacrylPOSS (POSS) from Hybrid Plastics; 3-(Trimethoxysilyl) propylmethacrylate 98% (TMMS), DCP from Alpha Aesar.

Compounding: SBR SLR 4630 from Styron Europe GmbH had 25 wt. % of styrene, 63 wt. % of vinyl groups and 37.5 phr of aliphatic extension oil; antioxidant *N*-(1,3-dimethylbutyl)-*N′*-phenyl-*p*-phenylendiamine (6PPD) Santoflex-6PPD was purchased from Flexsys; zinc oxide from Zincol Ossidi; stearic acid Stearina TP8 from Undesa.

2.2. Preparation and morphological characterization of SiO_2@POSS hybrid filler

SiO_2@POSS hybrid filler was prepared by the double-step functionalization procedure reported in the previous work [12]. Firstly, SiO_2 (30 phr, i.e. parts of hundreds of rubber) were functionalized with 20 wt.% of TMMS with respect to silica in a methanol/water solution (4/1 v/v); secondly SiO_2-TMMS NPs were suspended in toluene (150 mL) and then POSS nanounits (10 wt.%) were introduced into the solution in the presence of a suitable amount of DCP (2 wt.%, molar ratio POSS/DCP = 20/1). The peroxide promotes the activation of the methacrylate groups of both silane and POSS units, favoring the anchoring of the nanocages onto the silica surface and their partial condensation to form, possibly, nanometric networks [29].

Morphological characterization of SiO_2@POSS and SiO_2 TMMS powder was performed on a Jeol 3010 HRTEM operating at 300 kV with a high-resolution pole piece (0.17 nm point to point resolution) and equipped with a Gatan slow-scan 794 CCD camera.

Nitrogen physisorption measurements on SiO_2-TMMS and SiO_2@POSS hybrid filler were carried out by a Quantachrome Autosorb-1 apparatus [32,33]. The specific surface area (SSA_{BET}, BET method) was measured after evacuation at 150 °C for 16 h.

2.3. Preparation of uncured and cured nanocomposites

In order to prepare uncured rubber nanocomposites, SiO_2@POSS hybrid filler was mixed by *ex-situ blending* with SBR in a Brabender Plasti-corder lab station (mixing chamber of 50 mL, filling factor of 0.7) [12].

SBR polymer (32.0 ± 0.5phr) was first introduced into the mixer and plasticized for 30 s at 60 RPM at 145 °C, then 30phr of SiO_2-TMMS or 33phr SiO_2@POSS hybrid filler was introduced, mixed for about 4 min and then discharged.

Vulcanization chemicals were then added to the composites in two further steps. Firstly, stearic acid (2 phr), zinc oxide (3.5 phr) and 6-PPD (2 phr) were mixed with the obtained composites at 60 rpm for 5 min at 145 °C. Successively, DCP (1.5 phr) was introduced at a working temperature of 90 °C and by mixing at 60 rpm for 3 min.

Since both the filler networking and distribution are related to the DCP during the curing process, composites have been cured at different temperature. In detail, cured composites were obtained by vulcanization using a hydraulic press at 155 °C, 170 °C and 185 °C for 10 min running time under a pressure of 200 bar. Hereafter, cured nanocomposites are labelled as C-SBR/SiO_2@POSS_X where X refers to the different curing temperature.

In order to find a relation between the peculiar structure of the SiO_2@POSS hybrid filler and the features of the resulting composites, the properties of SBR/SiO_2@POSS, both uncured and cured, were compared to those of nanocomposites prepared by simply mixing SiO_2, TMMS and OctaMethacrylPOSS in the same polymer matrix, under the same experimental conditions (i.e. curing chemicals, temperature, rotor speed) described above.

Uncured and cured SBR/SiO_2 + POSS composites were prepared by blending SBR with a filler mixture composed by SiO_2 Rhodia (30 phr), a TMMS coupling agent (2 phr) and 10phr of OctaMethacrylPOSS. These composites, before and after curing, are labelled as SBR/SiO_2 + POSS and C-SBR/SiO_2 + POSS_X, respectively, where X refers to the different curing temperature. A reference material without any filler was prepared by the same experimental conditions (i.e. curing chemicals, temperature, rotor speed) described above. These composites, before or after curing, are labelled as SBR pure or C-SBR pure, respectively.

2.4. Morphological characterization of silica nanofillers and silica–SBR nanocomposites

Morphological study of both uncured and cured SBR/SiO_2@POSS and SBR/SiO_2 + POSS composites was carried out by Transmission Electron Microscopy (TEM) with a Zeiss EM 900 microscope working at an acceleration voltage of 80 kV. Ultrathin sections (about 50 nm thick) of composites were obtained with a Leica EM FCS cryo-ultramicrotome equipped with a diamond knife (samples kept at −130 °C).

Light microscopy (LM) was employed to visualize the overall morphology of the cured composites. Two LM microscopes were used: stereomicroscope SMZ-2T (Nikon) for the lowest magnifications and the highest depth-of-focus, and wide-field light microscope Nikon Eclipse 80i (Nikon) for higher magnifications up to 40 ×. The surface of the samples was observed directly in reflected light. Under these conditions, the micrographs showed brighter agglomerates of the fillers on darker background.

The investigation of the interfacial adhesion between hybrid nanofiller and rubber of the nanocomposites cured at different temperature was carried out by SEM using Microscope Quanta 200 FEG (FEI). The samples were fractured in liquid nitrogen, sputtered with a thin platinum layer (4 nm of Pt, deposited using vacuum sputter coater SCD 050 (Leica)) and observed at an accelerating voltage 30 kV using both secondary electrons detector (SE) and backscattered electrons detector (BSE). SE and BSE micrographs showed mostly topographic and material contrast, respectively.

The investigation of the topography and the heterogeneity relief was

done using an atomic force microscope (Dimension Icon, Bruker), equipped with a SSS-NCL probe, Super Sharp SiliconTM – SPM-Sensor (NanoSensorsTM Switzerland; spring constant 35 N m^{-1}, resonant frequency ≈ 170 kHz). The analysis was performed on fresh surfaces after freeze-fracturing the materials to obtain "cross-sectional images" under ambient conditions using the tapping mode AFM technique. In these conditions it is possible to investigate the topography and heterogeneity of the composite from the nano to micrometer level. The scans covered the sizes from 1 × 1 to 20 × 20 μm^2. Investigation on the crude materials was not possible because of their high stickiness.

2.5. Solid state NMR characterization of silica nanofillers and silica–SBR nanocomposites

High-resolution solid-state NMR spectra were recorded using a Bruker Avance III HD 500 WB/US NMR spectrometer (Karlsruhe, Germany, 2013) in a double-resonance 4-mm probehead. In all cases, the samples were placed into the thick-wall 4-mm ZrO_2 rotors (o.d.). The ^{13}C cross-polarization (CP) magic angle spinning (MAS) NMR spectra were recorded with a MAS frequency $\omega_r/2\pi$ = 11 kHz, $B_1(^{13}C)$ field nutation frequency of 62.5 kHz, a contact time of 1.75 ms and a repetition delay of 4 s. During the data acquisition, a high-power dipolar decoupling SPINAL64 was applied. The applied nutation frequency of $B_1(^1H)$ field for decoupling was $\omega_1/2\pi$ = 89.3 kHz. The decoupling flip-pulse length was 3.4 μs. The ^{13}C NMR scale was calibrated with glycine as an external standard (176.03 ppm – low-field carbonyl signal). The signal assignment was performed according to literature data. ^{1}H NMR spectra were recorded at the MAS frequency $\omega_r/2\pi$ = 15 kHz as well as under static conditions. The static ^{1}H NMR spectra were simulated, decomposed to individual spectral component in order to determine the amount of rigid domains and to probe degree of immobilization of polymer segment by determining signal linewidths. To compensate for frictional heating of the spinning samples, all NMR experiments were measured under active cooling. The sample temperature was maintained at 305 K. Precise temperature calibration was performed on $Pb(NO_3)_2$ using a calibration procedure described in literature [34].

Low-resolution solid-state NMR experiments were carried out on a Stelar PC-NMR spectrometer coupled with a Niumag permanent magnet working at a Larmor frequency of 20.8 MHz for ^{1}H nuclei. ^{1}H Free Induction Decays (FIDs) were recorded under on-resonance conditions by means of a solid echo pulse sequence, and short, solid-like spin-spin relaxation times were obtained by means of a discrete analysis of the FID. In order to obtain more accurate values of the weights of the FID components, Solid Echo (SE) measurements at different echo delays were performed within an echo delay range of 13–31 μs, and the weights obtained at the different delays were extrapolated to zero delay. Long, liquid-like spin-spin relaxation times were determined by means of the Carr-Purcell-Meiboom-Gill (CPMG) pulse sequence, using an echo delay of 13 μs. A relaxation delay of 1 s and 200 scans were always used. The temperature was always in the range 24–26° C. The 90° pulse duration was 3 μs.

2.6. Rheological analysis and tensile tests

Curing profiles were measured with a moving die rheometer (RPA 2000, Alpha Technological) under the following conditions: ± 1° oscillation angle, 155, 170 and 185 °C curing temperatures, 4.3 bar pressure and 10 min running time.

DMTA of C-SBR/SiO_2@POSS_X, C-SBR/SiO_2 + POSS_X, C-SBR/SiO_2-TMMS and C-SBR pure was performed by an Ares G2 apparatus (TA Instruments) by applying a shear stress mode. The temperature dependence of the complex shear modulus of rectangular samples (5 × 1 × 0.25 cm^3) was measured by oscillatory shear deformation at a frequency of 1 Hz and at the heating rate of 3 °C min$^-$Tensile tests were carried out using an Instron 5800 apparatus at 25 °C and a crosshead speed of 50 mm min^{-1}. For each sample, five dumbbell samples were tested and the average value was evaluated.

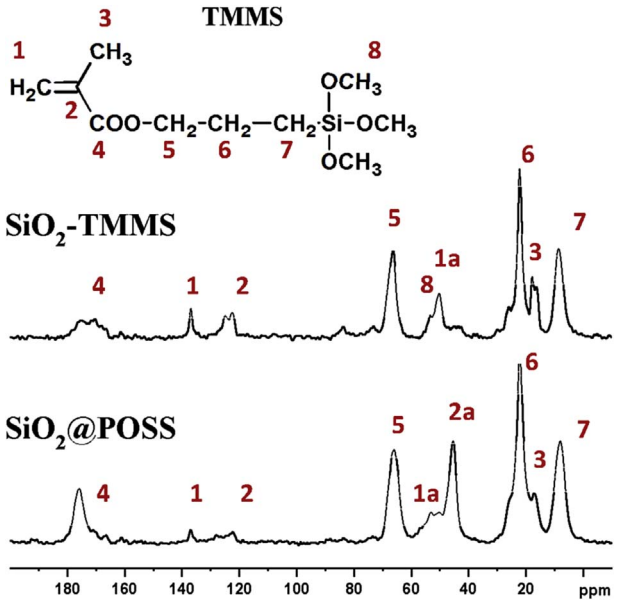

Fig. 1. ^{13}C CP/MAS NMR spectra of SiO_2-TMMS and SiO_2@POSS nanofillers.

3. Results and discussion

3.1. Spectroscopic and morphological characterization of SiO_2-TMMS and SiO_2@POSS hybrid nanofillers

The NMR and morphological characterizations of SiO_2-TMMS and SiO_2@POSS fillers reported in a previous paper [12] are here reproduced to more deeply discuss the capability of POSS anchored SiO_2 NPs in enhancing the nanocomposite mechanical properties, compared to the simple SiO_2 + POSS NPs.

Specifically, ^{13}C CP/MAS NMR spectroscopy was used to determine the organic composition of SiO_2-TMMS and SiO_2@POSS hybrid nanofiller, whose spectra with the labelling scheme and the signal assignment [34–36] are presented in Fig. 1, and discussed in comparison with the NMR spectrum of the pristine TMMS reported in our previous study [12].

In SiO_2-TMMS spectrum (Fig. 1 top) the signals due to the propylmethacrylate chains (5, 6, 7) are clearly detectable as well as the resonances 1 and 2 ascribable to the vinyl carbon (H_2C =) available for the further reaction with POSS. In the ^{13}C spectrum of SiO_2@POSS, the reaction between the acrylate functions of TMMS and POSS, activated by DCP, leads to the appearance of the peaks 2a at 45 ppm and 1a in the range 52–56 ppm, both attributed to -CH_2-based chains formed through polymerization. The downfield shift (of about 8 ppm) of the carbonyl peak 4, compared to the resonance found at 167.2 ppm in the unreacted acrylate chains of TMMS (see ref. 12), further confirms the successful polymerization. Finally, in SiO_2@POSS, weak signals in the range 110–150 ppm can be easily detected (signals 1 and 2 at 125.1 and 137.4 ppm, respectively), suggesting the presence of residual C=C bonds which should be available for the cross-linking reactions with rubber chains during the curing of the composites. Residual CH_3-O-groups reflected by very weak signals at ca. 50 ppm then indicate nearly complete hydrolysis of Si-O-CH_3 units.

As reported in the previous paper [12], TEM investigation showed that pure SiO_2-TMMS is constituted by large agglomerates, where the NPs are aggregated (Fig. S1a, Supporting Information). After functionalization with POSS units (SiO_2@POSS), the silica NPs boundaries appear less defined than in pure silica (Fig. S1b). This effect is related to the presence of POSS domains on the particle surface which, after

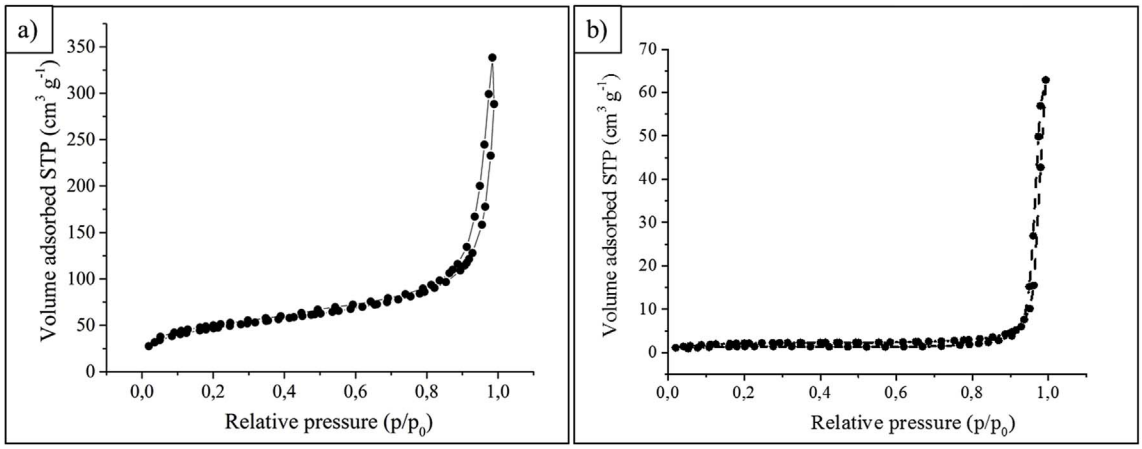

Fig. 2. Adsorption–desorption isotherm at liquid nitrogen temperature of: a) pristine SiO_2 and b) SiO_2@POSS hybrid nanofiller.

activation of the methacryl functionalities by DCP, may induce further NPs aggregation in the composite.

Nitrogen physisorption experiments were performed on bare SiO_2, SiO_2-TMMS and SiO_2@POSS nanoparticles in order to highlight the effect of functionalization on the aggregation/porosity of the fillers. In particular, the adsorption − desorption isotherms of pristine silica and SiO_2@POSS samples are reported in Fig. 2.

SiO_2 NPs display a type II Brunauer isotherm, typical of microporous materials, and a relatively high specific surface area (SSA_{BET}) of 168.6 ± 3.4 $m^2 g^{-1}$. Conversely, SiO_2@POSS shows a Type III isotherm, characteristic of non porous systems. Accordingly, a remarkable reduction of the surface area is detected for this sample (SSA_{BET} = 8.2 ± 0.2 $m^2 g^{-1}$). Similar behaviour was observed for SiO_2-TMMS NPs with SSA_{BET} = 29.0 ± 0.6 $m^2 g^{-1}$ (isotherm not shown) [32,33].

These results may be explained by the outgassing treatment at 150 °C undergone by the samples before the measurements (see Experimental). This thermal activation may promote partial reactivity among the methacryl functionalities of POSS units in SiO_2@POSS, thus increasing the aggregation and leading to large filler agglomerates, which reduce the specific surface area.

3.2. Morphological characterization of C-SBR/SiO_2@POSS and C-SBR/SiO_2+POSS nanocomposites

In order to provide a comprehensive overview on a large scale of the sample morphology, the characterization of SBR/SiO_2@POSS and SBR/SiO_2+POSS nanocomposites cured at 170 °C was performed by light microscopy (LM).

The images show that C-SBR/SiO_2@POSS_170 is constituted by very large agglomerates of micrometric dimensions, inhomogeneously distributed through the rubbery matrix (Fig. 3a), while C-SBR/SiO_2+POSS_170 is constituted by smaller aggregates, well dispersed in the polymer matrix (Fig. 3b). These results are in agreement with the previously reported TEM investigation [12].

Thus, LM investigation seems to confirm the suggestion that the hybrid SiO_2@POSS NPs promote the formation of a tight filler network which immobilizes the filler in rubber, affording relevant reinforcement. However, further evidence must be provided to shed light on the filler-rubber interactions occurring in the presence of SiO_2@POSS hybrid filler, and to their role in modulating the final composites properties.

With this aim, a careful characterization of C-SBR/SiO_2+POSS_170 and C-SBR/SiO_2@POSS_170 nanocomposites cured nanocomposites by SEM and AFM microscopy was performed, focusing on the study at the micro and nanoscale level of the adhesion and formation of rigid rubber domains at the interface between filler and rubber [16–19,37].

The samples were frozen rapidly in liquid nitrogen and cracked on a plane in order to investigate the surface structure of the sample along the fracture (i.e. freeze fracturing).

Fig. 4 reports the SEM images collected for the two composites. C-SBR/SiO_2+POSS_170 shows a sharper interface with evident boundaries between the two phases (Fig. 4a and inset), while C-SBR/SiO_2@POSS_170 exhibited a continuous surface (Fig. 4b). Moreover, SiO_2@POSS hybrid NPs appears to be covered by the polymer on the fractured surface, and the interfacial adhesion between the filler and the polymer seems to be enhanced.

Under the hypothesis that both the filler networking and the dispersion are related to the DCP-activated reactivity of POSS and TMMS functionalities [31], SEM images have been collected for composites cured at: i) 155 °C, temperature at which the peroxide is less reactive and the curing is at the early stages; ii) 170 °C, i.e. the optimum temperature for DCP activation and curing; iii) 185 °C, a temperature at which the peroxide is completely reacted [26] (see curing properties in Section 3.3 and Fig. S4 in Supporting Information).

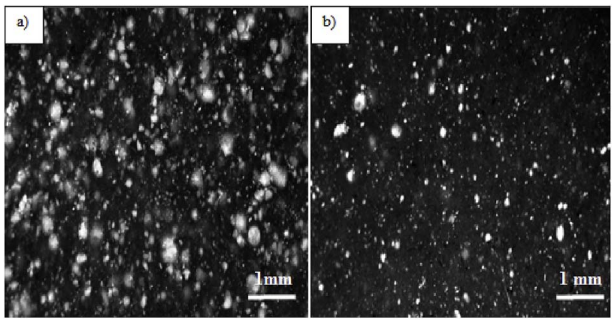

Fig. 3. LM images of a) SBR/SiO_2@POSS and b) SBR/SiO_2+POSS cured at 170 °C.

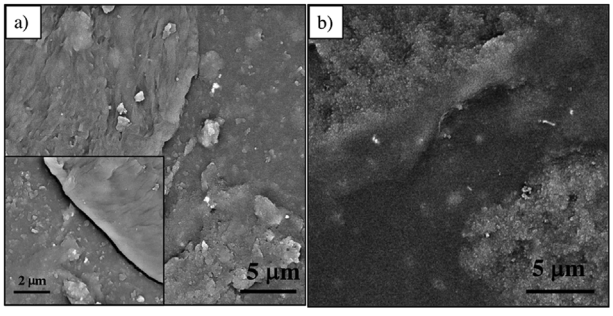

Fig. 4. SEM images at different magnifications of: a) C-SBR/SiO_2+POSS and b) C-SBR/SiO_2@POSS nanocomposites cured at 170 °C.

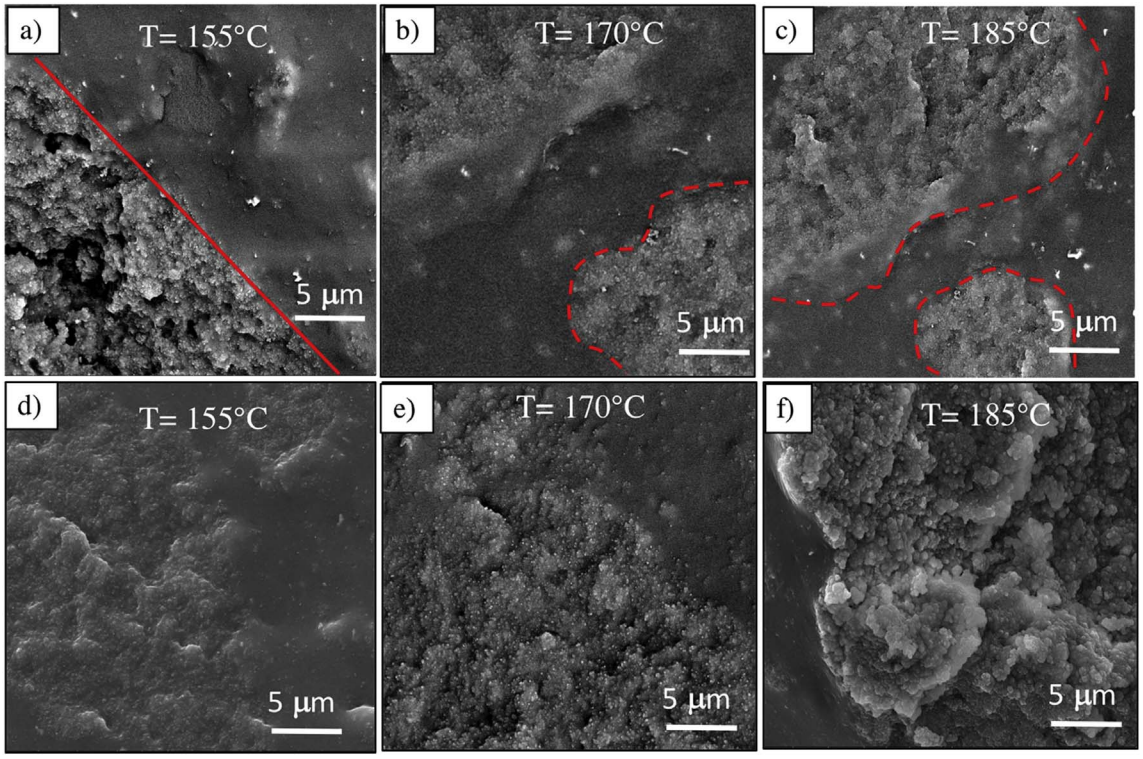

Fig. 5. a), b) and c) SEM images of C-SBR/SiO_2@POSS and d), e) and f) of C-SBR/SiO_2 + POSS cured at different temperatures (155, 170 and 185 °C).

The SEM micrographs of C-SBR/SiO_2 + POSS and C-SBR/SiO_2@POSS nanocomposites acquired at increasing curing temperature are summarized in Fig. 5. In detail, C-SBR/SiO_2@POSS_155 and C-SBR/SiO_2 + POSS_155 nanocomposites show sharp interfaces with significant boundaries between the two phases (Fig. 5 a, d). Moreover, the filler surface appears poorly penetrated by the rubber matrix, indicating weak adhesion between particles and polymer chains (Fig. 5 a, red line). This behaviour may be explained considering that, under these curing conditions, DCP is poorly active, and thus methacryl functionalities of both POSS and TMMS do not interact with the vinyl groups of SBR, causing weak filler-rubber interactions.

At 170 °C, i.e. the optimum activation temperature for DCP, the C-SBR/SiO_2 + POSS_170 nanocomposite show again phase separation and poor adhesion between filler and polymer (Fig. 5e). Instead, the C-SBR/SiO_2@POSS_170 sample exhibits continuous surfaces where the SiO_2@POSS hybrid nanofillers appear to be homogeneously covered by rubber, with remarkable interfacial adhesion (Fig. 5b dotted red line). This behaviour is more clearly detectable in the SEM images collected after curing at 185 °C (Fig. 5c dotted red line).

The overall SEM results show enhanced interfacial adhesion in SBR/SiO_2@POSS nanocomposites, suggesting a peculiar filler networking induced by the presence of the POSS nanounits, especially when they are grafted to silica in SiO_2@POSS, and mediated by DCP activation.

The interfacial adhesion, in term of rubber covering, of SBR/SiO_2@POSS nanocomposites subjected to different curing temperatures was also investigated by AFM operating in tapping mode in air, and reported in Fig. 6.

The image of C-SBR/SiO_2@POSS_155 composite (Fig. 6a), shows inhomogeneous dispersion of filler particles with small contact zone between the neighbour particles.

In the composite cured at 170 °C (conventional curing temperature), SiO_2@POSS NPs appear significantly aggregated and better covering of the filler (bright part) by rubber (dark part) is observed (Fig. 6b). Finally, in C-SBR/SiO_2@POSS_185, most of the filler particles are homogeneously covered by rubber (Fig. 6c). The AFM results, besides corroborating those obtained by SEM, suggest that the presence of SiO_2@POSS hybrid NPs actually generates a peculiar filler networking during the curing of the nanocomposites. This can be associated to the DCP-activated cross-linking action of the POSS nanocages anchored to SiO_2 NPs, which supplies remarkable compatibility with the polymer matrix and seems to favour rubber covering at the surface or even inside silica aggregates.

The AFM images of C-SBR/SiO_2 + POSS_X are reported in Fig. 6 (bottom). In these composites, silica NPs form small nanometric aggregates which are very uniformly dispersed in the matrix and only partially interconnected. This behaviour is clearly detectable in the images collected after curing at the highest temperatures (i.e. 170 °C and 185 °C). Moreover, by comparing the interfacial adhesion in C-SBR/SiO_2 + POSS_185 (Fig. 6f) with that in C-SBR/SiO_2@POSS_185 (Fig. 6c), it is evident a lower interaction between the filler and the rubber matrix for the composite obtained by simple mixing SiO_2, TMMS and POSS, as assessed by the prevalence of the bright spots in the images. This is in agreement with SEM results (Fig. 5b and c) and confirms the better adhesion between the two phases in SBR/SiO_2@POSS compared to SBR/SiO_2 + POSS (Fig. 5e and f) nanocomposites and, in turn, the key role of SiO_2@POSS NPs in the cross-linking action at the surface or even inside these aggregates.

3.3. *^{1}H solid-state NMR characterization of C-SBR/SiO_2@POSS and C-SBR/SiO_2 + POSS nanocomposites*

In order to investigate the dynamic properties of the rubber and, in particular, the immobilization of the rubber in proximity to the hybrid filler surfaces at the nanoscale level, a low-resolution solid state ^{1}H NMR study [11,20–27] was carried out, in analogy to SEM and AFM, on SBR/SiO_2@POSS and SBR/SiO_2 + POSS composites, the former also subjected to different curing temperatures.

The analysis of ^{1}H FIDs, recorded at low field under on resonance conditions by the solid echo (SE) [20] pulse sequence, by means of a nonlinear least squares fitting procedure, using a linear combination of suitable functions, allows the determination of the number and amount of domains with different degree of mobility present in a sample.

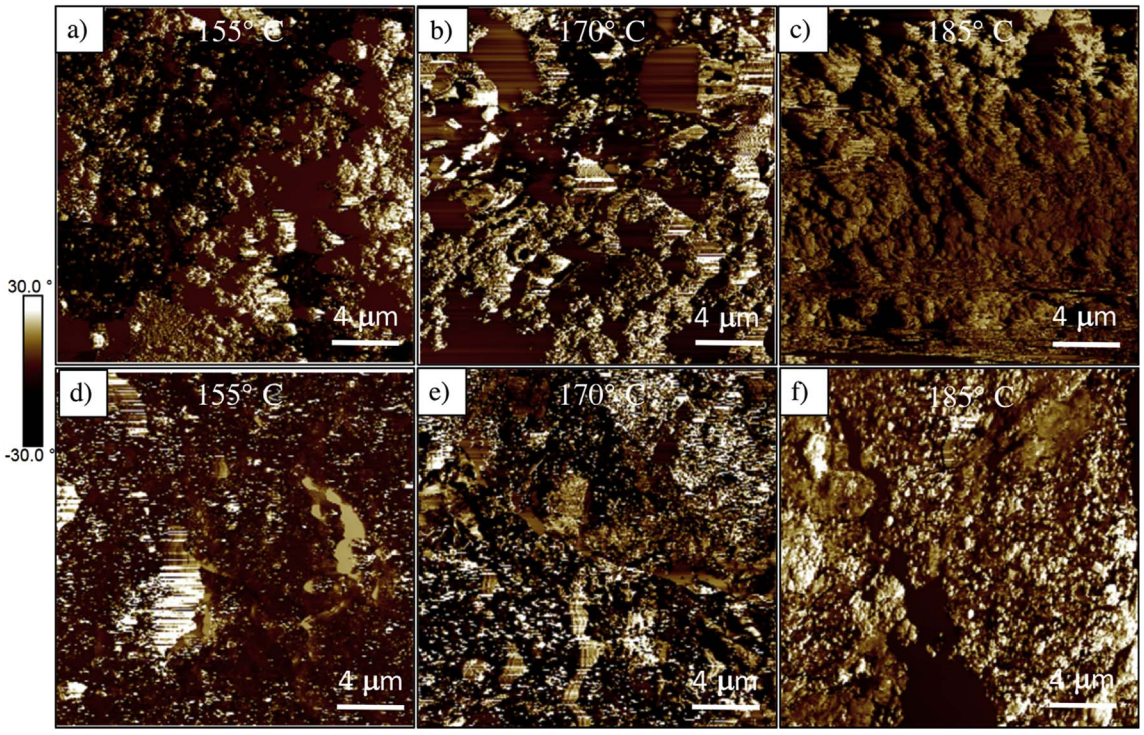

Fig. 6. a), b) and c) AFM images of C-SBR/SiO_2@POSS and d), e) and f) of C-SBR/SiO_2 + POSS cured at different temperatures (155, 170 and 185 °C).

The analytical function used in the FID fitting procedure can be written as:

$$F(t) = \sum_i w_i F_i(t, T_{2i})$$

where F(t) is normalized so as to be F(0) = 100.

The functions F_i which may be used to fit the FID are typically exponential, Gaussian, Weibullian, Pake and Abragamian. Each F_i is characterized by a different spin-spin relaxation time, T_{2i}, related to the molecular mobility of the system, and a weight percentage, w_i, ideally representing the percentage of protons belonging to the *i-th* domain.

For all the samples studied here, the best fits of the SE FIDs, recorded with an echo delay of 13 µs, were obtained using a combination of a Gaussian and two exponential functions (an example is shown in Fig. S2a).

The Gaussian spin-spin relaxation time, is always about 15–20 µs, a value typical of protons in very rigid domains. Therefore, the Gaussian component can be ascribed to all protons in the rigid environments present in the sample, either arising from the rubber or the filler. Regarding the two exponential functions, ^{1}H T_2's of about 100–130 and 440–500 µs were found for all the samples. Overall, they can be assigned to protons in more mobile environments and to the isolated hydroxyl groups of the filler.

However, since the SE technique is not ideal to determine long relaxation times, CPMG relaxation curves were also acquired. For all samples they were properly reproduced using a sum of three exponential functions, with corresponding T_2 of about 80–130 (exp1, weight ranging from 48 to 54%), 400–550 (exp2, weight of 17–33%) and 2500–3500 µs (exp3, weight of 2–4%) (an example is shown in Fig. S2b). These three exponential components gives a more reliable description of the non-rigid environments present in the samples. In particular, exp1 and exp2 are indicative of a distribution of mobile environments with slightly different mobility, mainly ascribable to the polymeric matrix, while exp3 can be safely assigned to polymeric free chain ends.

This interpretation is also supported by ^{1}H static spectra recorded at high magnetic field, reported in Fig. 7. Here, for all samples it can be observed a superposition of a broad signal resonating at about 4.6 ppm, arising from the rigid fractions of the samples and roughly corresponding to the Gaussian component of the FID, and three narrow lines, resonating at 7.0, 5.4, and 1.2 ppm, respectively ascribable to aromatic, unsaturated and saturated aliphatic protons belonging to the flexible fractions of the polymer, and roughly corresponding to the exponential components observed in the CPMG experiment. Typical decomposition of the static spectrum of C-SBR/SiO_2 + POSS system on the broad and narrow components including probehead background is demonstrated in the bottom part of Fig. 7.

In order to more reliably determine the weight of the Gaussian component found in SE FIDs, a procedure of extrapolation to zero echo delay was applied by fitting the trend of the intensities of the Gaussian and exponential components recorded at different values of the echo delay. Such procedure, applied to C-SBR-SiO_2@POSS_170, allowed us to determine suitable scaling factors to correct the weight percentages obtained from the fitting of the FID recorded with an echo delay of 13 µs: these scaling factors were also applied to the other samples, relying on the fact that all the FIDs were very similar. Gaussian weights ranging from 10 to 30% were obtained, reported in Table 1 along with the weights of the three exponential components found by the analysis of CPMG curves. Although the integrals of the ^{1}H static spectra recorded at high field are not strictly quantitative, the ratio between the integral of the broad signal at 4.6 ppm and the total integral of the spectrum (reported as supplementary information, Table S2) shows a trend similar to that of the Gaussian weight percentage obtained by ^{1}H FID analysis.

As previously stated, the weight percentage of the Gaussian component is ascribable to all the rigid components of the samples, including those contained in the filler. In order to separate the contributions from the rubber and filler, i.e. to determine the percentage of rigid rubber with respect to the total content of rubber, we further analyzed the experimental data using the following procedure: (a) a calibration curve ^{1}H solid echo signal intensity/sample weight vs. ^{1}H weight percentage was built using several weighted standard samples at known composition (see supplementary info – Table S1 and Fig. S3); (b) the ^{1}H weight percentage in the two pure fillers (SiO_2-TMMS and

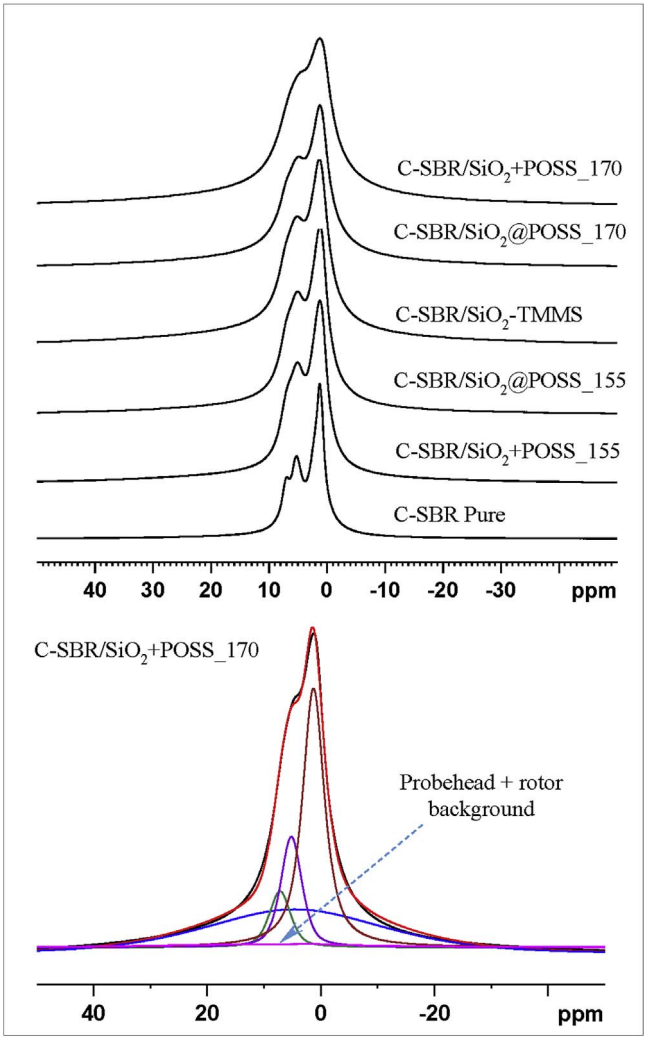

Fig. 7. Static ^{1}H NMR spectra of the C-SBR/SiO_2@POSS, C-SBR/SiO_2+ POSS C-SBR/SiO_2-TMMS composites and pure C-SBR cured at 170 °C. The spectrum of C-SBR/SiO_2@POSS_ 155 and C-SBR/SiO_2@POSS_155 are also reported for comparison. Bottom panel demonstrates decomposition of the static ^{1}H NMR spectrum of C-SBR/SiO_2+ POSS systems.

Table 1
Weights percentages (f_H%) of the different components of the fitting functions derived from the analysis of ^{1}H FID obtained by solid echo (for the Gaussian component and the sum of exponentials ones) and of the CPMG relaxation curves (individual exponential components).

Solid echo/CPMG f_H (%)				
Sample	Gau	exp1	exp2	exp3
C-SBR_170	10	53	33	4
C-SBR-SiO_2-TMMS	18	54	25	3
C-SBR-SiO_2@POSS_155	22	48	26	4
C-SBR-SiO_2@POSS_170	28	49	20	2
C-SBR-SiO_2@POSS_185	30	51	17	2
C-SBR-SiO_2 + POSS_170	23	50	23	3

SiO_2@POSS) was determined through the calibration curve, after measuring the ^{1}H solid echo signal intensity/sample weight for the pure fillers (see supplementary info – Table S3); (c) the proton fractions in rigid environments (Gaussian component) in the pure fillers was determined by ^{1}H FID analysis (see supplementary info – Table S3); (d) the contribution to the Gaussian component of the ^{1}H FIDs in nanocomposites arising from protons in the fillers was estimated knowing the amount of filler in the composites (35 phr) and assuming that the dynamic properties of the filler did not change in passing from the pure fillers to the nanocomposites; (e) the percentage of rigid rubber was obtained from the ^{1}H FID analysis by subtracting the contribution from the filler estimated at step (d). The procedure above described could be applied to all the investigated samples excluding C-SBR/SiO_2 + POSS, for which obviously the amount of protons in rigid environments of the filler could not be estimated.

Table 2
Percentage of ^{1}H nuclei (%H) in rigid environments, as determined by FID analysis using the procedure described in the text: fractions of total protons in rigid environments (f_{Hrigid}^{TOT}), of protons in rigid environments of the sole filler (f_{Hrigid}^{filler}), of protons in rigid environments of the sole rubber (f_{Hrigid}^{SBR}) relative to the whole nanocomposite, and fraction of protons in rigid environments of the sole rubber relative to the SBR component (f_{Hrigid}^{SBR*}).

Sample	%H (mol) relative to the composite			%H (mol) relative to SBR only
	f_{Hrigid}^{TOT}	f_{Hrigid}^{filler}	f_{Hrigid}^{SBR}	f_{Hrigid}^{SBR*}
C-SBR_170	10	–	–	10
C-SBR-SiO_2-TMMS	18	3	15	16
C-SBR-SiO_2@POSS_155	22	5	17	19
C-SBR-SiO_2@POSS_170	28	5	23	25
C-SBR-SiO_2@POSS_185	30	5	25	27
C-SBR-SiO_2 + POSS_170	23	–	–	–

The results are summarized in Table 2 and in Fig. 8. It can be observed that the amount of rigid rubber, (f_{Hrigid}^{SBR*} in Table 2), 10% in the pure rubber (cured at 170 °C), increases to 16% in C-SBR/SiO_2-TMMS and further to 19, 25 and 27% to C-SBR/SiO_2@POSS samples, cured at 155, 170, and 185 °C, respectively. This clearly indicates that the presence of the filler induces the formation of a remarkable amount (from 6 to 17%) of rigid rubber, in addition to that already present in the pure rubber.

Both the curing temperature and the filler type have a significant effect in determining the amount of rigid rubber present in the final material, being largest when POSS and the highest curing temperature are used. In particular, the total fraction of protons in rigid environments increases with the curing temperature, and is in C-SBR/SiO_2@POSS cured at 170 and 185 °C compared to C-SBR/SiO_2@POSS_155. A similar trend has been observed for SBR/SiO_2 + POSS nanocomposites (not shown). Interestingly, although the fraction of rigid rubber could not be accurately estimated for C-SBR/SiO_2 + POSS, the total fraction of rigid protons determined for this system (23%) was much lower than that of C-SBR/SiO_2@POSS cured at 170 and 185 °C.

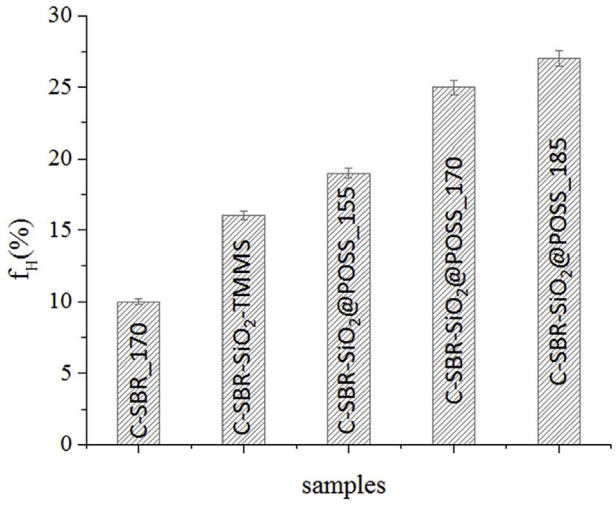

Fig. 8. Fraction of rigid rubber determined by ^{1}H FID analysis as described in the text.

The above results are in agreement with the morphological and adhesion properties of the composites. In particular, whilst C-SBR/SiO_2 + POSS samples display sharper interfaces with evident boundaries between the two phases, C-SBR/SiO_2@POSS composites exhibit continuous surfaces and the filler aggregates appear to be highly covered by the polymer (cfr. Figs. 4 and 5). This supports the remarkable immobilization of rubber chains (i.e higher amount of rigid protons) provided by SiO_2@POSS hybrid NPs assessed by NMR.

Finally, the lower restricted mobility determined for SBR/SiO_2@POSS sample cured at 155 °C, compared to those cured at 170 and 185 °C, strengthens the idea that, at the lowest temperature, the crosslinking between the methacryl groups of OctaMethacrylPOSS in SiO_2@POSS hybrid filler and rubber chains is weak, due to the ineffective activation of dicumylperoxide. Consequently, the network formation is hindered and very poor interfacial adhesion is detected (cfr. Figs. 5 and 6) until the curing temperature is raised to optimum (i.e. 170 and 185 °C), at which a gradual increase of the aggregation among SiO_2@POSS NPs probably occurs, leading to an enhanced rubber chains immobilization at the surface or even inside these aggregates.

3.4. Rheological properties and tensile tests

In order to get deeper insights into the influence of the peculiar structure of the SiO_2@POSS hybrid filler on the final composite properties, the curing profiles [38] and the mechanical features (DMTA analysis) of SBR/SiO_2@POSS and SBR/SiO_2 + POSS samples were determined [39–41].

The curing kinetic of the nanocomposites was studied by measuring the variation of viscosity with time, using the torque required to keep the rotor rate constant. To obtain more specific information, some useful physical parameters that can describe the structural characteristics of the rubber composites were extracted from the rheological curves: the minimum torque ML, i.e the torque measured at the scorch time t_{S1}, which is the time during which the rubber composite can be manipulated before curing; the curing time t_{MH}, i.e. the time required to completely cure the composite; the maximum torque MH, which is the torque measured when the reticulation can be considered complete.

In detail, SBR/SiO_2@POSS_170 sample shows higher torque value than SBR/SiO_2 + POSS_170 (Fig. S4 and Table 3), suggesting a larger degree of rubber reticulation induced by the presence of SiO_2@POSS hybrid filler. This is in agreement with the morphological and NMR results, pointing out that SBR/SiO_2@POSS nanocomposites exhibit the highest fraction of rigid domains and surface confined polymer chains.

As described above, the filler networking, interfacial adhesion and rubber immobilization in the composites are remarkably influenced by the curing temperature. Thus, curing curves were collected for composites cured also at 155 and 185 °C (Fig. S5). As expected, the maximum torque increases with the curing temperature and becomes maximum for the C-SBR/SiO_2@POSS_185 sample, which evidences also the lowest t_{MH}. This validates the hypothesis that, at 155 °C, the peroxide is actually less reactive and the curing is at the early stages, while at temperature above 170 °C DCP is fully reacted and the reticulation can be considered complete.

In order to study these effects in depth, DMTA analysis [35–37] was initially carried out on SBR/SiO_2@POSS and SBR/SiO_2 + POSS samples cured at 170 °C, i.e. the optimum temperature for DCP activation (170 °C). The obtained results are summarized in Fig. 9.

Table 3
Curing parameters for SBR nanocomposites.

Samples	Min torque (ML) (kPa)	Curing Time (t_{MH}) (min)	Max Torque (MH) (kPa)
C-SBR/SiO_2 + POSS_170	5.9	6.3	18.3
C-SBR/SiO_2@POSS_155	6.0	n.d.	19.7
C-SBR/SiO_2@POSS_170	6.0	8.2	27.2
C-SBR/SiO_2@POSS_185	6.2	4.1	27.7

In agreement with RPA measurements reported in our previous study, both C-SBR/SiO_2@POSS_170 and C-SBR/SiO_2 + POSS_170 induce in the rubbery state higher modulus in comparison to the composites containing exclusively silica and TMMS. Moreover, it must be observed that C-SBR/SiO_2@POSS exhibits better performance than C-SBR/SiO_2 + POSS nanocomposite (Fig. 9a) This again witnesses the better capability of the hybrid nanofiller in upgrading the mechanical properties of SBR.

The same experiments have been also performed on nanocomposites cured at 155 and 185 °C. The obtained results are summarized in Fig. 9b, which shows the trend of the storage modulus for SBR/SiO_2@POSS and SBR/SiO_2 + POSS nanocomposites as a function of the curing temperature. As expected, C-SBR/SiO_2@POSS_170 and SBR/SiO_2@POSS_185 display higher moduli in comparison to the composite cured at 155 °C. This suggests a gradual increase of aggregation among SiO_2@POSS NPs as the curing proceeds, leading to enhanced rubber chain immobilization at the surface or even inside these aggregates, in accordance with both morphological and NMR results.

Instead, a minor dependence of the storage modulus values on the curing temperature is observed for SBR/SiO_2 + POSS nanocomposites (Fig. 9b, blue-line). This behaviour may be ascribed to the competition in these materials, due to simply mixing silica, TMMS and POSS with SBR, of the following simultaneous interactions: (i) POSS-POSS, ii) POSS-TMMS, (iii) POSS-TMMS-Silica, (iv) POSS-SBR and (v) TMMS-SBR.

These concurrent phenomena lead to the presence of more dispersed and less compact filler aggregates weakly bonded with the polymer chains (see SEM/AFM microscopy and NMR investigation), resulting in G′ values still high but significantly lower than those of SBR/SiO_2@POSS nanocomposites cured under the same conditions.

Tensile tests were performed in order to further shed light on the effects of the POSS incorporation on rubber nanocomposite, by evaluating their behaviour under high deformation conditions [42]. Stress strain profiles for cured C-SBR/SiO_2@POSS_170 (red line), C-SBR/SiO_2 + POSS_170 (blue line), C- SBR/SiO_2-TMMS and C-SBR (black line) composites are reported in Fig. 10.

Cured SBR rubber (Fig. 10 black line) shows high extensibility and low modulus due to the absence of the filler. In this case, dicumylperoxide only activates the chain-chain cross-polymerization of vinyl groups of the rubber, thus resulting in a low crosslinking density and, consequently, in a low modulus and a high extensibility. Instead, the presence of SiO_2-TMMS filler leads to the rubber reinforcement but high extensibility is still found.

Interestingly, the behaviour of C-SBR/SiO_2@POSS_170 and C-SBR/SiO_2 + POSS_170 nanocomposites (Fig. 10, red line and blue line respectively) is remarkably different. In C-SBR/SiO_2@POSS_170 nanocomposite, the aggregates are covered by rubber layer, and the polymer chains are significantly immobilized, as determined by NMR. Accordingly, the composite shows the highest modulus and the lowest extensibility and toughness (Fig. 10, red line). The same experiments have also been performed on nanocomposites cured at 155 and 185 °C. As expected, the obtained results show a decrease in extensibility increasing the curing temperature (not shown).

Instead, in C-SBR/SiO_2 + POSS_170, POSS units are probably anchored to silica NPs with lower efficiency, and their grafting may occur only during the curing process. This leads to the presence of more dispersed filler aggregates, resulting only in a partial increase of the modulus and to a higher extensibility compared to C-SBR/SiO_2@POSS_170 (Fig. 10, blue line). Similar behavior has been observed for the other composites cured at 155 and 185 °C (not shown).

In order to better explain the above results, Fig. 11 shows a schematic proposal of the network influence on the tensile properties in C-SBR/SiO_2@POSS and C-SBR/SiO_2 + POSS nanocomposites.

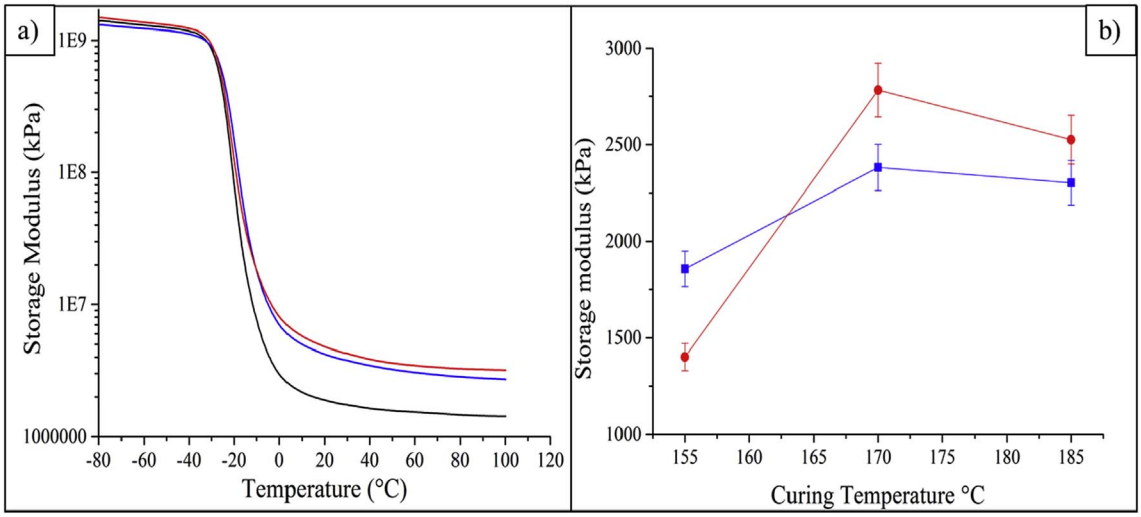

Fig. 9. Left side: plot of storage modulus G′ vs. temperature C-SBR (black line), SBR/SiO_2@POSS_170 (red line) and SBR/SiO_2 + POSS_170 (blue line) nanocomposites. Right side: details of the trend of G′ values as a function of the curing temperature for SBR/SiO_2@POSS (red line) and SBR/SiO_2 + POSS (blues line) nanocomposites.

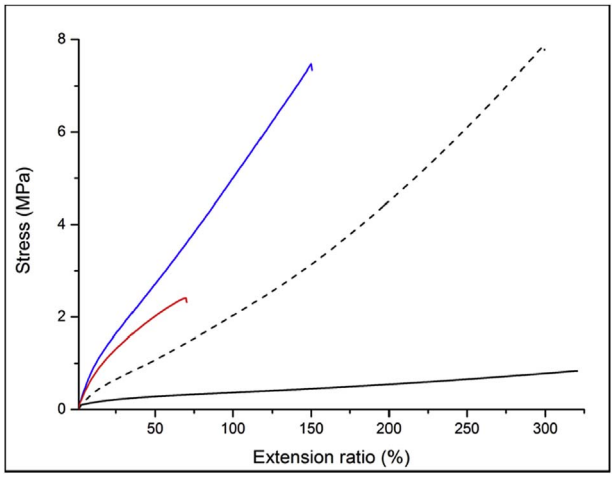

Fig. 10. Tensile Stress-strain profile for C-SBR/SiO_2@POSS_170 (red line), C-SBR/SiO_2 + POSS_170 (blue line), C-SBR/SiO_2-TMMS (dotted line) and C-SBR pure (black line) composites. (For interpretation of the references to colour in this figure legend, the reader is referred to the Web version of this article.)

In detail, the dumbbell samples represent the specimens utilized for the measurements; F is the force applied from the instruments until the breakdown of the samples. When F is applied, the variation in terms of network formation induces relevant differences in the extensibility properties.

The presence of a rigid filler network strongly bonded to the polymer in SBR/SiO_2@POSS nanocomposites reduces/prevents the elongation of the samples (Fig. 11, left-side) much more than in SBR/SiO_2 + POSS, where more dispersed and less compact filler aggregates in the sample (Fig. 11, right side).

The results indicate that the good adhesion between filler and polymer (i.e. the presence of a tight network immobilizing rubber chains) in SBR/SiO_2@POSS samples gives superior mechanical properties but, due to percolation, it contributes to the matrix brittleness inducing much lower extensibility than for SBR/SiO_2 + POSS composites.

3.5. Model for network formation in SBR/SiO_2@POSS nanocomposites

The morphological, spectroscopic and tensile results in total allowed us to propose a mechanism for the network formation in SBR/SiO_2@POSS nanocomposites during the curing reaction (Fig. 12).

In the early stages of the curing (i.e. at 155 °C), the crosslinking between the methacryl groups of POSS and rubber chains is limited, due to ineffective activation of dicumylperoxide. As a consequence, the filler networking is hindered and very poor interfacial adhesion is detected (see SEM and AFM investigation). Accordingly, low rubber chains immobilization is retrieved by NMR.

As the curing proceeds and the temperature is raised up to 170 °C or 185 °C, the full activation of DCP promotes the crosslinking reactions (green lines) involving the methacryl functionalities of POSS units grafted onto SiO_2 NPs. This leads to the generation of a percolating network constituted by large and compact (up to ~ 300 μm) interconnected aggregates, distributed inhomogeneously through the rubbery matrix and highly bound to the polymer phase. These conclusions are supported by SEM, AFM and ^{1}H NMR experiments, showing higher interfacial adhesion of the filler network with the polymer, better covering of the filler by rubber layers and higher restricted mobility of the rubber chains for SBR/SiO_2@POSS nanocomposites cured at 170 and 185 °C compared to C-SBR/SiO_2@POSS_155, respectively. As a result, the composites show high modulus and a relatively low extensibility and toughness due to the rigid filler network bonding to the rubber matrix.

Conversely, it is not an easy task to suggest a model for the network formation in C-SBR/SiO_2 + POSS nanocomposites, since along the curing competition between concurrent processes occurs. In detail, when POSS nanocages are not anchored to SiO_2 NPs like in SiO_2@POSS nanofiller, their simply mixing with TMMS and SBR may result in the following simultaneous interactions: (i) POSS-POSS, ii) POSS-TMMS, (iii) POSS-TMMS-Silica, (iv) POSS-SBR and (v) TMMS-SBR. These, besides favoring the networking, may favor covalent bonding between filler-rubber, resulting in the coverage of the aggregates by rubber layers, sterically restricting their further growth and their percolation in the polymer matrix.

Consequently, the C-SBR/SiO_2 + POSS composites displays a non percolating filler network, containing smaller filler aggregates (up to ~ 100 μm) better dispersed in a polymer matrix, which appears less efficient in immobilizing the rubber chains, as demonstrated by the lower fraction of rigid protons, the lower modulus and the significantly higher extensibility and toughness compared to C-SBR/SiO_2@POSS.

4. Conclusions

This study reports on the influence of hybrid SiO_2@POSS nanofiller, where silica NPs and POSS nanocages are intimately interconnected, on

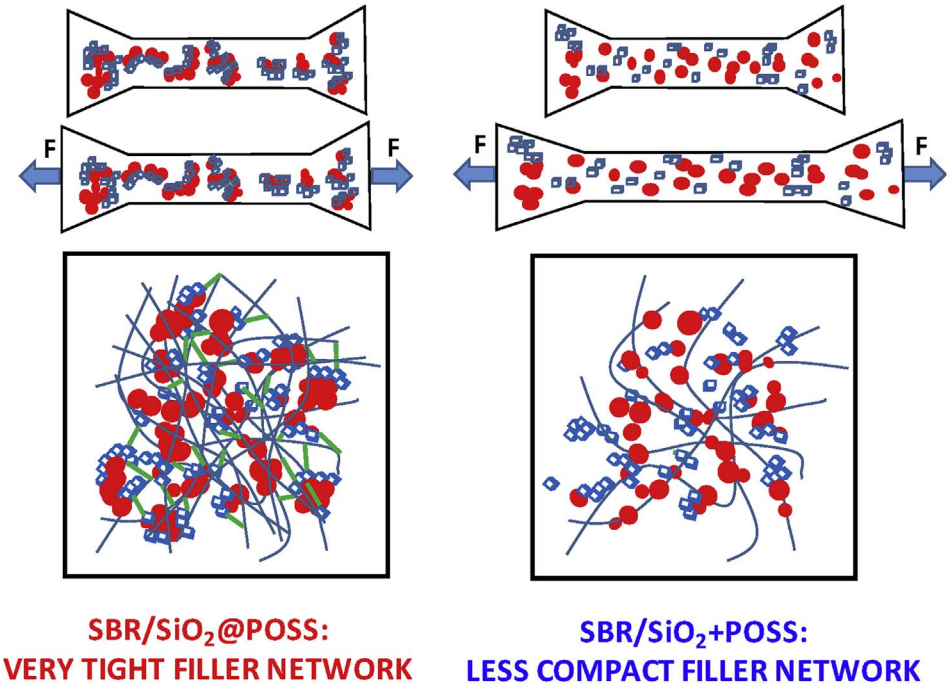

Fig. 11. Schematic of the effect of the filler network in SBR/SiO_2@POSS and SBR/SiO_2 + POSS nanocomposites on their extensibility. Red spheres stand for SiO_2 NPs, while blue cubes represent POSS units. Green lines indicated the crosslinking reaction between hybrid filler and SBR. (For interpretation of the references to colour in this figure legend, the reader is referred to the Web version of this article.)

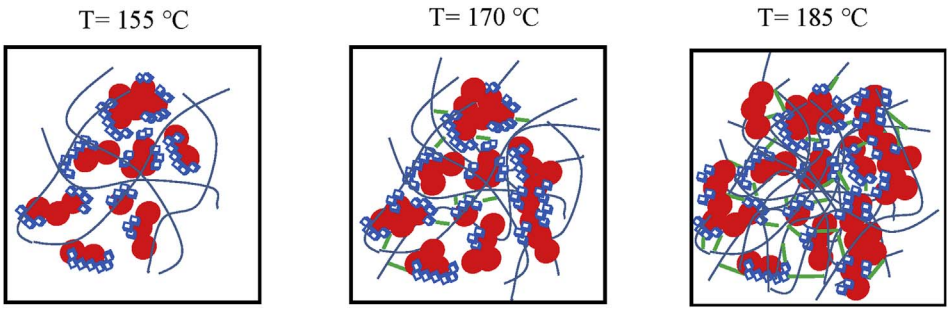

Fig. 12. Mechanism for the network formation in SBR/SiO_2@POSS nanocomposites during the curing process. Red spheres stand for SiO_2 NPs, while blue cubes represent POSS units. Green lines indicated the crosslinking reaction between hybrid filler and SBR. (For interpretation of the references to colour in this figure legend, the reader is referred to the Web version of this article.)

the properties at the micro and nanoscale level of SBR nanocomposites (i.e. C-SBR/SiO_2@POSS), focusing on the hybrid interface between the filler and the polymer. Moreover, a parallel comparison with C-SBR/SiO_2 + POSS system, obtained by simply mixing SiO_2, TMMS and POSS in SBR, has been provided.

In detail, the microscopic inspection of C-SBR/SiO_2@POSS nanocomposites, by means of SEM and AFM on fractured sections, revealed the occurrence of continuous surfaces with high interfacial adhesion between filler and rubber. Conversely, C-SBR/SiO_2 + POSS displays sharper interfaces and evident boundaries between the two phases, resulting in lower adhesion properties.

The immobilization of the rubber chains has been proved also at the nanoscale by solid state ^{1}H NMR, which unveiled for C-SBR/SiO_2@POSS a remarkable fraction of rigid protons close to the hybrid SiO_2@POSS surfaces. Instead, the total fraction of rigid protons resulted lower in SBR/SiO_2 + POSS suggesting a reduced amount of immobilized rubber chains.

These features induce better mechanical properties, lower extensibility and toughness in C-SBR/SiO_2@POSS compared to C-SBR/SiO_2 + POSS composites, as assessed by DMTA and tensile stress–strain tests, respectively.

As both the filler distribution and networking are clearly connected to the curing peroxide (DCP), which activates the POSS functionalities, these properties have been evaluated also after curing the composites at increasing temperatures, i.e. from when DCP is in principle less reactive and the curing process is at the early stages, toward the conditions where it is surely active and the curing is complete. It turned out that interfacial adhesion, rubber immobilization and storage modulus increase with the curing temperature and are higher for C-SBR/SiO_2@POSS cured at 170 and 185 °C than for C-SBR/SiO_2 + POSS obtained under the same conditions.

These results has been explained considering that, in these latter materials, competition between simultaneous interactions involving POSS nanounits (i.e. POSS-POSS, POSS-TMMS, POSS-TMMS-Silica, POSS-SBR and TMMS-SBR) may occur, resulting in highly dispersed and less compact filler aggregates weakly bonded to the polymer chains and, in turn, to a reduction of the mechanical properties.

The results in total allowed us to propose a model for the network formation in C-SBR/SiO_2@POSS.

This is based on the progressive activation by DCP of methacryl functionalities of POSS units which, intimately connected to SiO_2 NPs in SiO_2@POSS, enable the crosslinking reactions directly in proximity of the filler surfaces, leading to the generation of a tight network strongly bonded to the rubber chains.

Acknowledgements

This work was carried out in the frame of the European COST action MP1202 “Rational design of hybrid organic-inorganic interfaces: the next step towards advanced functional materials”.

M.R. thanks Corimav (“Consortium for the Research of Advanced Materials between Pirelli and Milano Bicocca University) for its support within the PCAM European Doctoral Programme.

Appendix A. Supplementary data

Supplementary data related to this article can be found at http://dx.doi.org/10.1016/j.polymertesting.2017.12.022.

References

[1] I. Mora-Barrantes, L. Ibarra, A. Rodrıguez, L. Gonzalez, J.L. Valentın, J. Mater. Chem. 21 (2011) 17526.
[2] T. Sabu, S. Ranimol, Rubber Nanocomposites: Preparation, Properties and Application, first ed., Wiley-Interscience, New York, 2010.
[3] G. Heinrich, M. Kluppel, A.T. Vilgis, Curr. Opin. Solid State Mater. Sci. 32 (2002) 195–203.
[4] E. Hall, J.C. Moreland, Rubber Chem. Technol. 74 (2001) 525–539.
[5] D. Goritz, H. Raab, J. Frohlich, P.G. Maier, Rubber Chem. Technol. 72 (1999) 929–945.
[6] J.B. Donnet, Compos. Sci. Technol. 63 (2003) 1085–1088.
[7] J. Frolich, W. Niedermeier, H.D. Luginsland, Composites, Part A 36 (2005) 449–460.
[8] J.L. Leblanc, Prog. Polym. Sci. 27 (2002) 627–687.
[9] L. Wahba, M. D'Arienzo, R. Donetti, T. Hanel, R. Scotti, L. Tadiello, F. Morazzoni, RSC Adv. 3 (2013) 5832–5844.
[10] R. Scotti, L. Conzatti, M. D'Arienzo, B. Di Credico, L. Giannini, T. Hanel, P. Stagnaro, A. Susanna, L. Tadiello, F. Morazzoni, Polymer 55 (2014) 1497–1506.
[11] L. Tadiello, M. D'Arienzo, B. Di Credico, T. Hanel, L. Matejka, M. Mauri, F. Morazzoni, R. Simonutti, M. Spirkova, R. Scotti, Soft Matter 11 (2015) 4022–4033.
[12] M. D'Arienzo, M. Redaelli, E. Callone, L. Conzatti, B. Di Credico, S. Dirè, L. Giannini, S. Polizzi, I. Schizzi, R. Scotti, L. Tadiello, F. Morazzoni, Mater. Chem. Front 1 (2017) 212–230.
[13] H. i Zhou, Q. Yea, J. Xu, Mater. Chem. Front. 1 (2017) 212–230.
[14] E. Ayandele, B. Sarkar, P. Alexandridis, Nanomaterials 2 (2012) 445–475.
[15] K.N. Raftopoulos, K. Pielichowski, Prog. Polym. Sci. 52 (2016) 136–187.
[16] S. Fu, X.Q. Feng, B. Lauke, Y. Mai, Composites: Part B 39 (2008) 933–961.
[17] S. Aoyama, T. Park, C.W. Macosko, T. Ougizawa, G. Haugstad, Langmuir 30 (2014) 12950–12959.
[18] X. Yong Gan, Int. J Mol Sci. 10 (2009) 5115–5134.
[19] a) S.C. Tjong, Mater. Sci. Eng. 53 (2006) 73–197;
b) M.Maiti and A. K.Bhowmick, Polymer, 47(2006) 6156–6166.
[20] E. Hansen, P. Kristiansen, B. Pedersen, J. Phys. Chem. B 102 (1998) 5444.
[21] V.M. Livtinov, Soliman, Polymer 46 (2005) 3077.
[22] V.M. Livtinov, J.P. Penning, Macromol. Chem. Phys. 205 (2004) 1721.
[23] B. Meissner, Rubber Chem. Technol. 68 (1995) 297–310.
[24] J. Brus, M. Urbanová, A. Strachota, Macromolecules 41 (2008) 372–386.
[25] J. Brus, M. Urbanová, I. Kelnar, J. Kotek, Macromolecules 39 (2006) 5400–5409.
[26] J. Brus, J. Dyba, Polymer 41 (2001) 5269–5282.
[27] V.M. Litvinov, P.A. M Steeman, Macromolecules 32 (1999) 8476–8490.
[28] L. González, A. Rodríguez, A. Marcos, C. Chamorro, Rubber Chem. Technol. 69 (1996) 203–214.
[29] G. Tsagaropoulos, A. Eisenberg, Macromolecules 28 (1994) 6067–6077.
[30] G. Tsagaropoulos, A. Eisenberg, Macromolecules 28 (1996) 396–398.
[31] N. Tsubokawa, H. Ishida, J. Polym. Sci. Part A: Polym. Chem. 30 (1992) 2241–2246.
[32] M. Crippa, E. Callone, M. D'Arienzo, K. Mu¨ller, S. Polizzi, L. Wahba, F. Morazzoni, R. Scotti, Appl. Catal. B Environ. 104 (2011) 282–290.
[33] S. Brunauer, P.H. Emmet, E. Teller, J. Am. Chem. Soc. 60 (1938) 309.
[34] J. Brus, Solid State Nucl. Magn. Reson. 16 (2000) 151–160.
[35] R. Di Maggio, E. Callone, F. Girardi, S. Dirè, J. Appl. Polym. Sci. 125 (2012) 1713–1723.
[36] F. Graziola, F. Girardi, R. Di Maggio, E. Callone, E. Miorin, M. Negri, K. Muller, S. Gross, Prog. Org. Coating 74 (2012) 479–490.
[37] V. Mittal, Characterization Techniques for Polymer Nanocomposites, Wiley, 2012.
[38] A. Susanna, L. Armelao, E. Callone, S. Dirè, M. D'Arienzo, B. Di Credico, L. Giannini, T. Hanel, R. Scotti, F. Morazzoni, Chem. Eng. J. 275 (2015) 245–252.
[39] L. Matějka, I.A. Kroutilová, J.D. Lichtenhan, T.S. Haddad, Eur. Polym. J. 52 (2014) 117–126.
[40] G. Maier, D. Goritz, G.K. Kautsch, Polymer 118 (1996) 5134–5135.
[41] A.P. Meera, J. Phys. Chem. C 113 (2009) 17997–18002.
[42] Brush Performance Alloys, Technical Tidbits, (2011).